Anharmonic Protein Motions and Heme Deformations in Myoglobin Cyanide Probed by Absorption and Resonance Raman Spectroscopy

**Reinhard Schweitzer-Stenner,*,†,‡ Antonio Cupane,§ Maurizio Leone,§ Christina Lemke,†
Joachim Schott,† and Wolfgang Dreybrodt†**

*FB1–Institut für Experimentelle Physik, Universität Bremen, 28359 Bremen, Germany, Department of
Chemistry, University of Puerto Rico, P.O. Box 23346, San Juan, PR00931, USA, and Istituto Nazionale di
Fisica della Materia and Dipartimento di Scienze Fisiche e Astronomiche, Universita di' Palermo,
90123 Palermo, Italy*

The Soret absorption of myoglobin cyanide in a 65% glycerol/water mixture was measured as a function of temperature between 20 and 300 K. The data were analyzed by using an earlier model relating each transition into the vibronic manifold of the electronic B-state to a Voigtian band profile (Cupane et al. *Eur. Biophys. J.* **1995,** *23,* 385, 1995). Its Gaussian part contains a temperature-dependent component due to the coupling of low-frequency modes to the Soret transition. The analysis of the vibronic substructure was facilitated by comparison with vibronic coupling parameters derived from the line intensities in the polarized Raman spectra taken with Soret excitation. From the depolarization ratios of several Raman lines, the existence of asymmetric heme macrocycle distortions was inferred, which lift the degeneracy of the excited B state. Raman intensities and depolarization ratios were then analyzed by a theory that formulates the polarizability tensor in terms of a time-independent perturbation theory. The vibronic coupling parameters thus obtained are linearly related to normal coordinate deformations of the heme macrocycle. The results obtained from this analysis of the Raman data suggest a Soret band splitting of ca. 130 cm^{-1}. This finding was then explicitly taken into account in the analysis of the Soret band absorption. The temperature dependence of the Gaussian broadening was found to deviate from the predictions of a harmonic model above a temperature that is slightly lower than the glass temperature of the glycerol/water solvent. This clearly indicates the onset of anharmonic motions within the protein environment, which are coupled to out-of-plane vibrations of the central iron atom. At room temperature, the degree of anharmonicity is much larger than that observed for myoglobin carbonmonoxide and is comparable with that of deoxymyoglobin. This indicates that oxidation and the spin state of the central iron atom have a significant impact on its dynamic properties. From the analysis of the depolarization ratio dispersion and the resonance excitation profiles of the oxidation marker band, we infer a rhombic distortion of the heme group that gives rise to nonequivalent Fe–N distances. Finally, the appearance of polarized Raman lines arising from A_{2u} type vibrations indicates that the heme group is somewhat domed despite its hexacoordinated state.

Introduction

It is now widely accepted that an in-depth understanding of proteins requires a detailed knowledge of the relationship between structure, function, and dynamics. At ambient temperature, the latter is governed by thermally driven motions over barriers between several conformational substates (CS) constituted by different orientations of amino acid residues as well as by protein segments with slightly different backbone conformations.[1]

In the case of heme proteins, the research focuses on the structural dynamic of the functional heme group to explore its dependence on specific heme–protein interactions. In this context, absorption spectroscopy has been proven well suited for probing the coupling of low-frequency protein modes to electronic transitions of the heme macrocycle.[2] For the intense Soret band, this vibronic interaction gives rise to a temperature-dependent Gaussian broadening. It convolutes with the natural Lorentzian bandwidth and a temperature-independent Gaussian part, which reflects static inhomogeneity for all Franck–Condon allowed transitions into the vibronic manifold. Experiments on various heme proteins in a water–glycerol mixture have shown that above a distinct temperature, which in some cases coincides with the glass temperature of the solvent, the thermal broadening of optical absorption becomes significantly larger than that predicted by a harmonic oscillator model.[3] This was interpreted as resulting from the onset of anharmonic protein motions between different CS, which are coupled to the heme group.[2,4] It was further shown that the central metal atom is pivotal for transducing the anharmonicity of the protein motions to the porphyrin macrocycle.[5,6]

To investigate the influence of the iron's spin state and electronic configuration on the heme, Leone et al. compared the temperature dependence of absorption spectra from low-spin heme proteins such as MbCN and HbCN with that obtained for deoxyMb and MbCO.[7] Surprisingly, this yielded unusually large vibronic coupling constants for the low-frequency mode

---

  * To whom correspondence should be addressed. Tel. 787-764-0000 (Ext: 2417). Fax: 787-759-6885. E-mail: stenner@web.uprr.pr.
  † Universität Bremen.
  ‡ University of Puerto Rico.
  § Universita di' Palermo.

Anharmonic Protein Motions and Heme Deformations

J. Phys. Chem. B, Vol. 104, No. 19, 2000 **4755**

ν_8 at 350 cm^{-1} for MbCN. This was tentatively explained by interpreting the corresponding coupling constant as an effective value that reflects a cluster of Raman active modes between 300 and 400 cm^{-1} as obtained for cytochrome *c*.[8]

This result demonstrates the necessity to employ resonance Raman spectroscopy for an independent check of the vibronic coupling parameters obtained from fitting the vibronic part of the Soret band. This has successfully been done in a recent study on metal−octaethylporphyrin in organic solvents.[9] The temperature dependence of spectral broadening also revealed a strong coupling to a bath of low-frequency modes with significant deviations from harmonic behavior above the glass transition temperature of the solvent. The strength of anharmonicity was found to strongly depend on the choice of the metal, that is, it is negligibly small for Cu(II), intermediate for Co(II), and very pronounced for Ni(II) and Pd(II).[9b] Altogether, these results point to a similarity between the dynamic properties of liquids and proteins, in accordance with the interpretation of neutron scattering data by Doster and co-workers.[10]

In the present study, we return to the investigations of Fe−porphyrins (heme groups) in proteins. We now utilize resonance Raman data to reanalyze the temperature dependence of the Soret band of ferric MbCN. To this end, absorption-corrected Raman spectra taken with Soret excitation were employed to determine the relative values of the Franck−Condon coupling constants for all intense A$_{1g}$-type bands (i.e., ν_2, ν_4, ν_7, ν_8) and also of bands from substituent modes that become Raman active by vibrational mixing with macrocycle vibrations. Next, the depolarization ratios and the excitation values of structure-sensitive marker bands with frequencies between 1300 and 1700 cm^{-1} for different excitation wavelengths in the Soret band region were determined to obtain information about symmetry-lowering distortions imposed by the axial ligands.[11] These data were subjected to an analysis based on a theory that formulates the Raman tensor by a nonadiabatic perturbation approach.[12] This yielded information about the splitting of B$_x$ and B$_y$ due to electronic and vibronic perturbations, which were then used to analyze the Soret band profile. By comparison with earlier results from various NMR,[13] electron spin−echo spectroscopy,[14] and polarized absorption spectroscopy on single crystals,[15] we were able to assess the heme distortions derived from the Raman data. The temperature dependence of the Soret band's Gaussian broadening was also reanalyzed and compared with that of deoxyMb and MbCO.

Theoretical Background

A. Raman Scattering. A detailed description of the Raman theory employed to analyze resonance excitation profiles (REPs) and the depolarization ratio dispersion (DPD) are given in ref 12b. In the present paper, the approach is simplified for the exclusive consideration of B-state excitation.

First-Order Vibronic Coupling and Selection Rules. The vibronic wave functions of porphyrins can be described by a third-order nonadiabatic perturbation expansion of a crude Born−Oppenheimer basis.[12] The first-order expansion coefficients reflect vibronic coupling between different excited electronic states |*l*> and |*m*>, that is,

$$c_{lm}^{\Gamma_r} = \left\langle l \left| \frac{\partial \hat{H}_{el0}}{\partial q_r^{\Gamma_r}} \right| m \right\rangle \langle 1 | q_r^{\Gamma_r} | 0 \rangle \tag{1}$$

where $q_r^{\Gamma_r}$ denotes the normal coordinate of the Raman vibration. $\partial \hat{H}_{el0}/\partial q_r^{\Gamma_r}$ is the vibronic coupling operator, Γ_r is the irreducible representation of the Raman vibration, and

$\langle 1 | q_r^{\Gamma_r} | 0 \rangle$ is its transition matrix element for the electronic ground state. In first order, the Raman cross section of a distinct mode is linearly dependent on the square of its matrix elements $c_{lm}^{\Gamma_r}$.[12b]

The electronic wave functions of the porphyrin electronic states involved in resonance Raman scattering can be expressed in terms of Gouterman's four-orbital model.[16] It is based on the assumption that the symmetry of the porphyrin macrocycle is D_{4h} and yields the 2-fold degenerated excited singlet states |B> =|B$_x$,B$_y$> and |Q> = |Q$_x$,Q$_y$>. The ground state is a singlet state of A$_{1g}$ symmetry. The electronic transitions |g>→|Q> and |g>→|B> give rise to the well-known Q and B bands in the optical spectrum.

Since |Q> and |B> transform like the irreducible representation E$_u$ of the D_{4h} point group, group theory dictates that $\Gamma_\rho = \Gamma(\partial \hat{H}_{el0}/\partial q_r^{\Gamma_r}) = \Gamma(q_r^{\Gamma_r}) = $ A$_{1g}$, B$_{1g}$, B$_{2g}$ or A$_{2g}$ for the symmetry of Raman active vibrations. Experimentally, Raman lines resulting from these vibrations can be distinguished by measuring their depolarization ratio, which is defined as

$$\rho = \frac{I_\perp}{I_\|} \tag{2}$$

where $I_\|$ *and* $I_\perp$ denote the scattered intensities measured parallel and perpendicular to the polarization of the exciting laser beam. In solution, the values for the above symmetries are 0.125 for A$_{1g}$, 0.75 for B$_{1g}$ and B$_{2g}$ and infinite for A$_{2g}$.[11]

Electronic Perturbations. Deviations from these depolarization ratio values are indicative of symmetry-lowering distortions, which may result from peripheral substituents, axial ligands, and heme−protein contacts.[11−14] Such asymmetric perturbations cause mixing of the electronic states and under some circumstances a lifting of the Q- and B-state degeneracy.[16,17] Theoretically, this can be accounted for by expanding the electronic Hamiltonian $\hat{H}(q, Q)$ with respect to the *static normal coordinate deformations* (SNCD) $\partial \bar{q}_a^{\Gamma_a}$ of the porphyrin's electronic ground state,[18] which are classified in terms of irreducible representations Γ_a of the D_{4h} point group.[11] As shown in ref 12b, this leads to the following matrix elements for A$_{1g}$ and B$_{1g}$ perturbations of the electronic structure:

$$\delta_{A_{2g}} = \langle Q_x | \hat{H}_{A_{1g}} | B_x \rangle = \langle Q_y | \hat{H}_{A_{1g}} | B_y \rangle$$

$$\delta_{B_{1g}} = \langle Q_x | \hat{H}_{B_{1g}} | B_x \rangle = -\langle Q_y | \hat{H}_{B_{1g}} | B_y \rangle \tag{3}$$

where $\hat{H}_\Gamma = \sum_j (\partial \hat{H}_{el0}/\partial q_j^{\Gamma_j}) \delta \bar{q}_j^{\Gamma_j}$. For the sake of simplicity, we neglect intramanifold electronic coupling in the 50:50 basis. Higher-order terms would account for out-of-plane distortions.[12b]

In the following, we confine ourselves to the vibronic B states because our experimental data were obtained solely with Soret excitation.[19] To account for the interactions described by eq 3, new electronic wave functions have to be derived that are written as a linear combination of the 50:50 states. The corresponding eigenenergies of |B$_x$> and |B$_y$> are written as[17]

$$E_{Bx} = \frac{E_B + E_Q}{2} + \sqrt{\frac{(E_B - E_Q)^2}{4} + (\delta_{A_{1g}} + \delta_{B_{1g}})^2}$$

$$E_{By} = \frac{E_B + E_Q}{2} + \sqrt{\frac{(E_B - E_Q)^2}{4} + (\delta_{A_{1g}} - \delta_{B_{1g}})^2} \tag{4a-b}$$

Equations 4a-b show that B$_{1g}$ perturbations lift the degeneracy of the B state.

Vibronic Perturbations. The above SNCDs also affect the vibronic states within a given electronic state and the vibronic coupling properties of the Raman active modes. This can be accounted for by expanding the vibronic coupling operator in eq 1 with respect to $\delta\bar{q}_j^{\Gamma_j}$. This yields

$$\frac{\partial\hat{H}_{el}}{\partial q} = \frac{\partial\hat{H}_{el0}}{\partial q_r^{\Gamma_r}} + \sum_{\Gamma_j}\sum_j \frac{\partial^2\hat{H}_{el0}}{\partial q_r^{\Gamma_r}\partial q_j^{\Gamma_j}}\delta\bar{q}_j^{\Gamma_j} \quad (5)$$

Term 1 reflects vibronic coupling in an undistorted D_{4h} symmetry. The influence of symmetry-lowering distortions is accounted for by the second term. To couple states of E_u symmetry, the product representation $\otimes$ of the latter must contain A_{1g}, B_{1g}, B_{2g} or A_{2g}.

The consequences for the symmetry of the Raman tensor can be deduced from eq 5 as follows. Let us consider a Raman active mode with A_{1g} symmetry in the undistorted molecule. If A_{1g} and B_{1g} perturbations are present,[20] the corresponding second terms in eq 4 will transform like A_{1g} and B_{1g}, whereas the first one will exhibit A_{1g} symmetry. As a consequence, the Raman tensor for B-band scattering has $A_{1g} \oplus B_{1g}$ symmetry and is therefore written as

$$\hat{\alpha} = \begin{bmatrix} (c_{BB}^{A_{1g}} + c_{BB}^{B_{1g}})M_{gB_x}^{\ 2} & 0 & 0 \\ 0 & (c_{BB}^{A_{1g}} - c_{BB}^{B_{1g}})M_{gB_y}^{\ 2} & 0 \\ 0 & 0 & 0 \end{bmatrix} \times$$
$$F_{BB}(\Omega_{exc}, \Omega_r^B, E_{B_x}, E_{B_y}) \quad (6a)$$

where[21,22]

$$c_{BB}^{A_{1g}} = \left\langle B_{x,y}\left|\frac{\partial\hat{H}_{el0}}{\partial q_r^{A_{1g}}} + \sum_j \frac{\partial^2\hat{H}_{el0}}{\partial q_r^{A_{1g}}\partial q_j^{A_{1g}}}\cdot\delta\bar{q}_j^{A_{1g}}\right|B_{x,y}\right\rangle\langle 1|q_r^{A_{1g}}|0\rangle$$

$$c_{BB}^{B_{1gr}} = \left\langle B_{x,y}\left|\sum_j \frac{\partial^2\hat{H}_{el0}}{\partial q_r^{A_{1g}}\partial q_j^{B_{1g}}}\cdot\delta\bar{q}_a^{B_{1g}}\right|B_{x,y}\right\rangle\langle 1|q_r^{A_{1g}}|0\rangle \quad (6b)$$

$M_{gB\sigma}(\sigma = x, y)$ are the dipole matrix elements, $F_{BB}(\Omega_{exc}, \Omega_r^B, E_{B_x}, E_{B_y})$ are frequency functions depending on the excitation energy, the frequency of the Raman mode in the excited B state(s), and the relative energies of B_x and B_y, respectively. Note that the z-component of the tensor is zero, since dipole transitions perpendicular to the heme plane are not considered.

Out-of-plane distortions may also induce Raman activity of out-of-plane vibrational modes via the first-order term of eq 5. A_{1u}-modes, for instance, may become Franck−Condon (FC) active with B-band excitation in the presence of A_{1u}-distortions, since in this case $\Gamma_r = A_{1u}$ and $\Gamma_j = A_{1u}$ so that $\Gamma_r = A_{1u} \otimes A_{1u} = A_{1g}$. Bands from such out-of-plane modes indeed appear in the low-frequency part of the Raman spectrum and will be discussed in detail below.

We now turn back to the Raman tensor in eq 5. In the presence of B_{1g} perturbations, the tensor elements α_{xx} and α_{yy} are no longer identical. As a consequence, the depolarization ratio (eq 2) deviates from its D_{4h} value of 0.125.

Vibronic coupling changes the eigenenergies of the excited vibronic states. Assuming again that A_{1g} and B_{1g} distortions are operative, the eigenenergies of the vibrational ground states of $|B_x\rangle$ and $|B_y\rangle$ are formulated in the second order of a nonadiabatic perturbation theory to yield[12b]

$$E_{B_x}' = E_{B_x} + \sum_\lambda\left[\frac{\Omega_\lambda}{2} - \frac{(c_{BB}^{A_{1g}}(\lambda) + c_{BB}^{B_{1g}}(\lambda))^2}{\Omega_\lambda}\right]$$

$$E_{B_y}' = E_{B_y} + \sum_\lambda\left[\frac{\Omega_\lambda}{2} - \frac{(c_{BB}^{A_{1g}}(\lambda) - c_{BB}^{B_{1g}}(\lambda))^2}{\Omega_\lambda}\right] \quad (7)$$

where E_{Bx} and E_{By} are the pure electronic energies of the perturbed molecule. Apparently, further splitting of $|B_x\rangle$ and $|B_y\rangle$ may be caused in by intrastate B_{1g}-type coupling.

Inserting the actual values of vibronic coupling parameters obtained from the fittings to the measured DRDs and REPs of the various modes (see below) and as reported in Table 2, one sees that, in the case of MbCN, vibronic contributions to the $B_x - B_y$ splitting are much smaller than the electronic ones (eq 4a and 4b).

Multimode Mixing. The theory discussed so far only describes first-order contributions to resonance Raman scattering, which only involves the creation of one Raman active vibration. In reality, multimode mixing may significantly contribute to the scattering cross section. It can be accounted for by expanding the vibronic wave functions into third order, which yields a somewhat lengthy expression for the Raman tensor components.[12] In this context, we confine ourselves to B-state intramanifold scattering. This yields a simpler expression for the Raman tensor, that is:

$$\hat{\alpha} = \begin{bmatrix} c_{BB}^+(r)M_{gB_x}^{\ 2} & \\ & c_{BB}^-(r)M_{gB_y}^{\ 2} \end{bmatrix}F^{(3)}_{BB}(\Omega_{exc}, \Omega_r^B, E_{B_x}, E_{B_y}) +$$
$$\sum_{\{\lambda\}}\begin{bmatrix} c_{BB}^+(r)c_{BB}^+(\lambda)c_{BB}^+(\lambda)M_{gB_x}^{\ 2} & 0 \\ 0 & c_{BB}^-(r)c_{BB}^-(\lambda)c_{BB}^-(\lambda)M_{gB_y}^{\ 2} \end{bmatrix} \times$$
$$F^{(5)}_{BB}(\Omega_{exc}, \Omega_r^B, \Omega_\lambda^B, E_{B_x}, E_{B_y}) \quad (8)$$

where r labels the vibration involved in Raman scattering and λ is a general label for a second mode, which contributes to Raman scattering via multimode mixing. The sum $\sum_{\{\lambda\}}$ runs over all permutations of matrix element combinations, as described in ref 13. The vibronic coupling matrix elements in eq 8 are defined as follows:

$$c_{BB}^\pm(j) = c_{BB}^{A_{1g}}(j) \pm c_{BB}^{B_{1g}}(j), j = r, \lambda \quad (9)$$

The frequency function $F^{(3)}_{BB}(\Omega_{exc}, \Omega_r^B, E_{B_x}, E_{B_y})$ of the first term is identical to that used in eq 6a. $F^{(5)}_{BB}(\Omega_{exc}, \Omega_r^B, \Omega_\lambda^B, E_{B_x}, E_{B_y})$ is a frequency function, which results from the third order of the perturbation approach and accounts for additional resonance positions due to excited vibronic states of the λ-th vibration.

Inhomogeneous Broadening. The temperature-independent inhomogeneous broadening was obtained from absorption spectra taken at low temperatures and was explicitly considered in the final calculation of the Raman cross section. The mathematics is given in ref 12b.

B. Optical Absorption Analysis. In the following, we briefly introduce the theory used to analyze the Soret band of MbCN. More details are given in ref 2. Our model is based on the assumption that vibronic transitions into the B-state manifold can be described in terms of the crude Born−Oppenheimer approximation. We described the Soret band by two series of vibronic bands due to the Franck−Condon-type transitions into the two lowest vibronic B_x and B_y-states, which are separated by Δ_B; the B_x−B_y splitting is given by the parameter Δ_B. The

Anharmonic Protein Motions and Heme Deformations

J. Phys. Chem. B, Vol. 104, No. 19, 2000 **4757**

latter was assumed to be temperature-independent. Furthermore, we considered several "high frequency" modes of the porphyrin macrocycle, as well as a bath of low-frequency modes that can be related to the phonon spectrum of the protein−solvent matrix.[9] As a consequence, the apparent profiles of all B_x- and B_y-bands are Voigtian and read as

$$A_\sigma(\nu) = M_{gB_\sigma}^2 \nu [L_\sigma(\Omega_{abs}, E_{B\sigma}) \otimes G_\sigma(\Omega_{abs}, E_{B\sigma})] \quad (10)$$

where $M_{gB}(\sigma = x,y)$ is a constant proportional to the electronic dipole matrix element, Ω_{abs} denotes the frequency position, and $L(\Omega_{abs})$ is the Lorentzian part of the band shape, which can be written as

$$L_\sigma(\Omega_{abs}) = \sum_{\{m_j\}} \left\{ \left[\prod_{j=1}^{N_h} \frac{S_j^{m_j} e^{-S_j}}{m_j!} \right] \cdot \frac{\Gamma}{\left(E_{B_\sigma}(T) + \sum_{j=0}^{N_h} m_j \Omega_j - \Omega_{abs}\right)^2 + \Gamma^2} \right\} \quad (11)$$

Γ is a damping factor, which depends on the finite lifetime, and the dephasing of the excited state and N_h denotes the number of high frequency modes vibronically coupled to the electronic transition. The product extends to all high-frequency porphyrin vibrations ($h\nu_j > k_BT$, where k_B denotes the Boltzmann constant, $\nu_i = c\Omega_j$), which are Franck−Condon active in the B state. The sum runs over all the possible combinations of occupation numbers m_j. Vibronic coupling of the "high frequency" porphyrin modes to the electronic transition is described by the linear coupling constants S_j, which for A_{1g}-type modes relates to the above introduced vibronic coupling matrix element $c_{BB}^{A_{1g}}$ by:[9a]

$$S_j = \left(\frac{(c_{BB}^{A_{1g}})_j}{\Omega_j} \right)^2 \quad (12)$$

Thus far, we neglected the influence of Jahn−Teller (JT) B_{1g}-type coupling which, however, may contribute due to a distortion of the same symmetry. As shown in the previous section, the respective electronic perturbation splits the x and y components of the vibronic states. The corresponding vibronic perturbation causes opposite displacements of the B_x and B_y potentials along the normal coordinate of the considered A_{1g} mode, that is, $\Delta_{B_x}^{A_{1g}}(c_{BB}^{B_{1g}}) = -\Delta_{B_y}^{A_{1g}}(c_{BB}^{B_{1g}})$. The total displacement is $\Delta_{B_x}^{A_{1g}}(c_{BB}^{A_{1g}}) + \Delta_{B_x}^{A_{1g}}(c_{BB}^{B_{1g}})$ for B_x and $\Delta_{B_x}^{A_{1g}}(c_{BB}^{A_{1g}}) - \Delta_{B_x}^{A_{1g}}(c_{BB}^{B_{1g}})$ for B_y. As a consequence, the S values are different for the two B states and are read as

$$S_{j,,x} = \left(\frac{(c_{BB}^{A_{1g}})_j + (c_{BB}^{B_{1g}})_j}{\Omega_j} \right)^2$$

$$S_{j,,y} = \left(\frac{(c_{BB}^{A_{1g}})_j - (c_{BB}^{B_{1g}})_j}{\Omega_j} \right)^2 \quad (13)$$

As shown in previous papers,[2,4,5] the B-state transition is also vibronically coupled to a "bath of low frequency modes" ($h\nu < k_BT$) described by an Einstein oscillator model which, in the short time limit, yields a Gaussian broadening of the Soret band and is described by the second term, $G(\nu)$, in eq 10:

$$G_\sigma(\Omega_{abs}) = \frac{1}{\sigma(T)} \exp\left[-\frac{(\Omega_{abs} - E_{B_\sigma}(T))^2}{2\sigma^2(T)} \right] \quad (14)$$

where $\sigma(T)$ is the temperature-dependent halfwidth. "Low frequency modes" are those whose vibrational energy is of the same order of, or smaller than, k_BT. Consequently, transitions from excited vibrational states are no longer negligible. As demonstrated by Melchers et al.,[6] these modes can be assigned mainly to the low-frequency part of the protein spectrum.

If one considers the above low-frequency bath as a set of N degenerate harmonic oscillators with an average coupling constant S and an average frequency $\langle\Omega\rangle$ (harmonic Einstein approximation), the temperature dependence of the Gaussian width (parameter $\sigma(T)$ in eq 14) is given by

$$\sigma_h^2(T) = NS\langle\Omega\rangle^2 \coth\left[\frac{hc\langle\Omega\rangle}{2k_BT} \right] + \sigma_{in}^2 \quad (15)$$

The subscript "h" indicates that eq 15 is only valid in the harmonic regime. The term σ_{in} accounts for an eventual temperature-independent inhomogeneous broadening, modeled as a Gaussian distribution of 0→0 transition frequencies.

Material and Methods

Materials. Horse heart metmyoglobin (metMb) was purchased from Sigma Chemie and dissolved in 0.1 M potassium phosphate buffer adjusted to pH 7. To obtain MbCN, the metMb sample was centrifuged, dissolved in a 65% v/v water/glycerol mixture, and allowed to react with a 2-fold molar excess of KCN. The concentration was adjusted to 0.66 mM for the Raman and to 10^{-5} M for the absorption measurements.

Optical Absorption Spectroscopy. Spectra in the range between 500 and 300 nm were recorded in digitized form at 0.5-nm intervals with a PC−IBM controlled Cary Varian 2300 spectrophotometer. The scan speed was 0.5 nm/sec, the integration time was 1 s, and the slit width was less than 0.4 nm in the whole wavelength range, corresponding to a spectral resolution of about 25 cm^{-1} at 400 nm.

Absorption measurements at various temperatures (300 to 20 K) were performed with MbCN dissolved in a 65% v/v mixture of glycerol and water, as described in detail by Cordone et al.[23] Samples were cooled with a rate of 1.5 K/min and were kept at each temperature for equilibration. Thermal cycling yielded fully reproducible results. The baseline (cuvette + solvent) measured at 300 K was subtracted from the spectra; in fact, it has been shown that in the wavelength region 500−380 nm, the baseline does not depend on temperature.

Resonance Raman Spectroscopy. The polarized Raman spectra of MbCN were measured with 413, 420, 425, 430, and 435 nm excitation by using a Krypton Ion Laser (Coherent, Innova 90 K) for 413-nm excitation and an excimer pumped dye laser (Lambda Physics) for the remaining wavelengths. Details of the experimental set up are given in reference 24.

Analysis of Raman Spectra. All spectra were subjected to a line shape analysis by the recently developed program MULTIFIT.[24] All spectra were corrected for self-absorption. The relative intensities I_{rel} of the bands in the polarized Raman spectra were calculated from band areas and used to determine the depolarization ratios with an accuracy of ±0.01. Possible systematic errors due to the finite collection angle for the scattered light are negligibly small.[25]

The weak but still detectable 1471 cm^{-1} band of glycerol was used to normalize the intensities of the Raman lines investigated. It was not possible to dissolve $NaClO_4$ in the water/glycerol mixture in a sufficient amount to use its polarized 934 cm^{-1} Raman line as an internal standard.
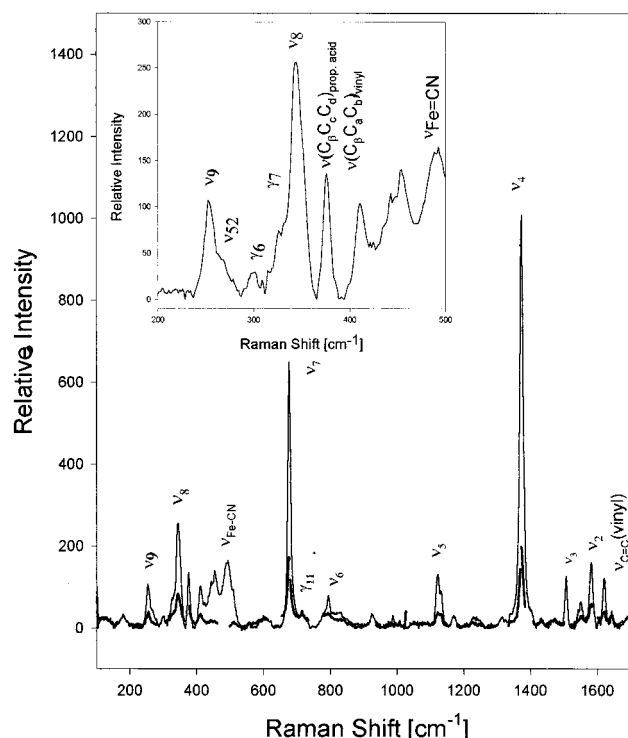
Figure 1. Polarized Raman spectra of MgCN taken with 425-nm excitation of an excimer pumped dye laser (average laser power 200 mW, spectral resolution 4 cm^{-1}). The low frequency part is enlarged in the inset. The spectrum was subjected to a band shape analysis.

A self-consistent analysis of the depolarization ratios and excitation profiles was carried out by adopting the protocol described in ref 12.

In earlier papers, we utilized a simple version of the transform theory to analyze Soret band Raman scattering.[9] The advantage of this method is that multimode mixing is implicitly taken into account.[26] However, it is difficult to apply if asymmetric distortions are operative. As we will show for MbCN, the presence of B$_{1g}$ distortions give rise to a B-band split into two separated bands with different band shapes. Without knowledge of these bands, the transform theory cannot be utilized. This prompted us to use our more traditional perturbation approach to determine the coupling strength of the investigated Raman lines, even though its iterative character makes this a somewhat more time-consuming procedure.

Results

Resonance Raman Data. Figure 1 shows the absorption-corrected polarized Raman spectra of MbCN taken with 425-nm excitation. We performed a self-consistent spectral analysis of these and other spectra measured at 413, 420, 430, and 435 nm. All bands could be well fitted with Lorentzian line shapes. The frequencies and assignments of all relevant lines are listed in Table 1. Their frequency positions are diagnostic of a hexacoordinated low spin state of the Fe^{3+}.

The overcrowded region between 200 and 500 cm^{-1} deserves some further comments. By comparison with most recent Raman studies on ferrocytochrome c,[8] myoglobin,[27] and cytochrome c peroxidase,[28] we identify polarized bands from out-of-plane and peripheral substituent modes besides the well-known A$_{1g}$-type macrocycle modes ν_8(343 cm^{-1}) and ν_9 (253 cm^{-1}). This comprises the A$_{2u}$-type modes γ_6(343 cm^{-1}) and γ_7 (299 cm^{-1}),[29] the structure-sensitive $\delta(CC_cC_d)$ bending mode of the proprionate groups, and the vinyl bending mode $\delta(CC_bC_a)$ at
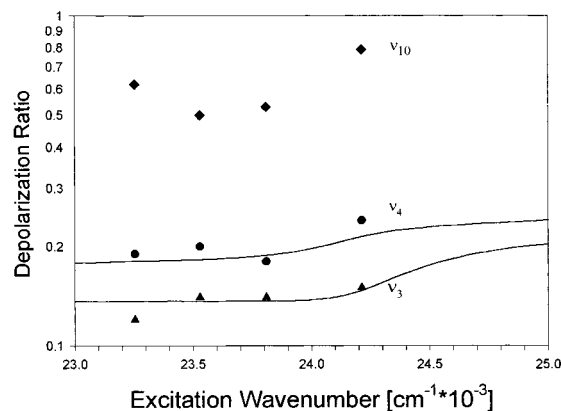
Figure 2. Depolarization ration of ν_3, ν_4, and ν_{10} observed with different Soret excitation wavelengths.

411 cm^{-1}.[30] Bands from the E$_u$-modes ν_{52} and ν_{48} are identified at 269 and 357 cm^{-1}.[8,27] Recently, evidence has been provided that the latter is mixed with the ligand FeCN deformation mode.[31] The quite broad band at 455 cm^{-1} results from the Fe$-$CN stretching mode. Another band of an out-of-plane mode is observed at 714 cm^{-1}, which, due to Hu et al.,[27] is assignable to the B$_{1u}$ mode γ_{11}. It appears nearly depolarized ($\rho = 0.5$), in contrast to the polarized bands of γ_6 and γ_7. The appearance of out-of-plane vibrations has some consequences for the understanding of the heme structure, which will be discussed below.

We have determined the depolarization ratios of the bands arising from the A$_{1g}$ modes. In Figure 2, the corresponding values for ν_3, ν_4, and ν_7, and the B$_{1g}$ mode ν_{10} are plotted as a function of the excitation wavelength. Depolarization values for ν_2m ν_7, and the low-frequency bands between 300 and 400 cm^{-1} are similar to respective values of ν_4 and are therefore not shown. With the exception of ν_3, the depolarization ratio of all lines deviate significantly from their D_{4h} value. First of all, this shows that asymmetric distortions are operative. Second, the data suggest that these distortions must be strong compared to those obtained earlier for other heme proteins, because it is experimentally established that for A$_{1g}$-type modes, symmetry-lowering deformations normally give rise to a dispersion of their depolarization ratios in the Q-band region, while they only slightly deviate from 0.125 with Soret excitation.[11,12b,32] This stems from the overwhelming scattering amplitude of FC-type scattering.

Figure 3 exhibits the obtained resonance excitation profile (REP) of ν_2, ν_4, ν_7, and the integrated intensity of the low-frequency bands between 300 and 400 cm^{-1}. The solid, dashed, solid$-$dashed, and dotted lines in Figures 2 and 3 result from self-consistent fits obtained as described in the Materials and Methods section. The fit was based on the assumption that the deviation of the depolarization ratios from their D_{4h} value of 0.125 is predominantly caused by B$_{1g}$-type distortions which, as we have shown in the theory section, give rise to a B$_{1g}$-type admixture to the Raman tensor (eqs 6a,b and 8). This is justified as follows. A$_{2g}$-type contributions can be ruled out because they are very unlikely to become significant in the B-band region.[12b] Admixture of B$_{2g}$-type coupling is possible, but the corresponding distortions would also cause an admixture of A$_{2g}$ symmetry to the Raman tensor of the B$_{1g}$ mode ν_{10}. Thus, the depolarization ratio should vary between 0.75 and ∞.[32] The corresponding experimental data in Figure 2, however, display instead the depolarization ratio between 0.5 and 0.75, which is diagnostic of an A$_{1g}$-type admixture and a B$_{1g}$ distortion. Finally, polarized absorption spectra on MbCN-crystals by El Naggar et al. are indicative of a comparatively strong Q-band splitting,[33]
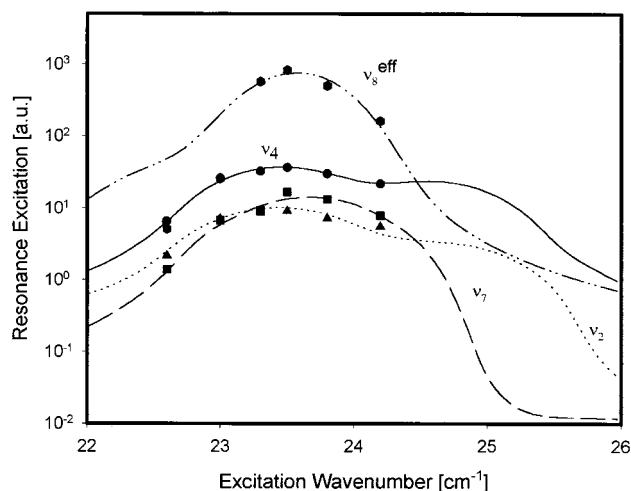
Anharmonic Protein Motions and Heme Deformations

J. Phys. Chem. B, Vol. 104, No. 19, 2000 **4759**

Figure 3. REPs of the Raman lines ν_2, ν_4, and ν_7 and of the integrated intensity of the spectral region between 300 and 400 cm^{-1}. The solid, dashed, dashed-dotted, and dotted lines result from the self-consistent fit described in the results section.

TABLE 1: Assignment of All Relevant Bands Appearing in the Raman Spectrum of MbCN

frequency [cm^{-1}]	assignment
253	$\nu_9(A_{1g})$
267	$\nu_{52}(E_u)$
327	$\gamma_7(A_{2u})$
343	$\nu_8(A_{1g})$
351	$\nu_{50}(E_u)$
375	$\delta(C_\beta C_c C_d)$ proprionic acid
410	$\delta(C_\beta C_a C_b)$ vinyl
455	Fe-CN s
676	$\nu_7(A_{1g})$
714	$\gamma_{11}(B_{1u})$
1374	$\nu_4(A_{1g})$
1506	$\nu_3(A_{1g})$
1581	$\nu_2(A_{1g})$
1590	$\nu_{19}(A_{2g})$
1620	C=C s vinyl
1642	$\nu_{10}(B_{1g})$

TABLE 2: Vibronic Coupling Parameters Expressed in Units of cm^{-1} Derived from the Self-Consistent Fit to DRDs and REPs of ν_2, ν_3, ν_4, ν_7 and the Integrated Intensity of the 300−400 cm^{-1} Region

	$c_{BB}^{A_{1g}}$ [cm^{-1}]	$c_{BB}^{B_{1g}}$ [cm^{-1}]
300−400 cm^{-1}	234	−75
ν_7	144	−49
ν_4	312	196
ν_3	123	7
ν_2	164	120

which normally results from B_{1g} rather than from B_{2g} distortions.[11,12b]

The vibronic and electronic coupling parameters obtained are listed in Tables 2 and 3. As one would expect from the depolarization ratios, intrastate B_{1g}-type coupling is relatively strong. This can be judged by the ratio $c_{BB}^{B_{1g}}/c_{BB}^{A_{1g}}$ of ν_4, which in the Soret band region predominantly determines the deviation of the depolarization ratio from its ideal D_{4h} value of 0.125. It is 0.63 for MbCN (Table 3), whereas values of 0.25 and 0.26 have earlier been obtained for deoxyMb and oxyMb, respectively.[34]

Absorption Data. Figure 4 illustrates our analysis of the Soret absorption spectrum of MbCN measured at 20 K. In accordance with the information derived from our Raman data, the Soret

TABLE 3: Electronic Parameters Express in Units of cm^{-1} as Derived from the Fit to DRD and REP of ν_2, ν_3, ν_4, ν_7 and the Integrated Intensity of the 300−400 cm^{-1} Region and the Optical Absorption Spectrum

parameter	value
E_B	2300[a]
Γ_B	230[a]
$\delta_{A_{1g}}$	−660[b]
$\delta_{B_{1g}}$	300

[a] Obtained from the Soret band shape analysis. [b] A guess, by comparison with other hexacoordinated heme proteins.
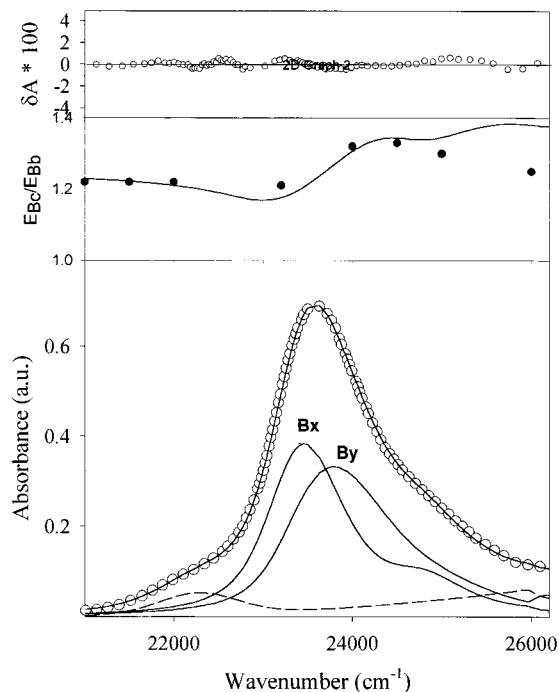

Figure 4. Soret band of MbCN recorded at 20 K. Circles are the experimental points; to improve figure readability, not all the experimental points have been reported. The band shape was decomposed into two equally intense components (solid lines) separated by 120 cm^{-1}, which are assignable to the electronic dipole transition into the split $|B_x\rangle$ and $|B_y\rangle$ states. The two smaller Gaussian bands on the high and low energy side (broken lines) are attributed to the N band of the heme group and to a charge transfer band, respectively; they have been subtracted from the spectra prior to the analysis. The residuals between the experimental points and the fitted band profile are depicted in the upper panel on an expanded scale. The intermediate panel compares experimentally observed values of the ratio of polarized absorption on a single MbCN crystal along its *b* and *c* axis from ref 15 with a theoretical calculation based on the present analysis. of B-band absorption in solution.

band is assumed to split into two bands, B_x and B_y, which are about 120 cm^{-1} apart. The splitting arises predominantly from pure electronic contributions (eq 4a,b) and is assumed to be independent of temperature. The vibronic B_{1g}-type contributions give rise to significant different intensities of B_x and B_y, and the ratio E_{Bx}/E_{By} is therefore strongly wavelength-dependent. This can easily be verified by inserting eq 13 into eq 11. The two broad and smaller bands on the high and low energy side of the Soret band are attributed to the *N* band of the heme group and to a charge-transfer band, respectively.[7] In the fit, we considered the coupling of both B_x and B_y with several high-frequency A_{1g}-type modes of the heme macrocycle, that is, ν_2 at 1581 cm^{-1}, ν_4 at 1374 cm^{-1}, ν_7 at 676 cm^{-1}, and ν_8 at 350 cm^{-1}. The S_{xj} and S_{yj} values obtained from the fits to the absorption and Raman data are listed in Table 4. Corresponding values agree within their limits of accuracy. This underscores

4760 *J. Phys. Chem. B, Vol. 104, No. 19, 2000*

Schweitzer-Stenner et al.

TABLE 4: Coupling Values S_{jx} and S_{jy} Obtained from the Vibronic Coupling Parameters (cf. eqs 13) in Table 2 and from the Global Fit to the Optical Absorption Spectra[a]

	Raman data				
	300−400	ν_7	ν_4	ν_3	ν_2
S_{xj}	0.2	0.02	0.14	0.007	0.011
S_{yj}	0.78	0.9	0.01	0.006	0.005

	Optical data		
	300−400	ν_7	1300−1600
S_{xj}	0.23	0.04	0.17
S_{yj}	0.86	0.10	0.09

[a] It is impossible to discriminate between the high frequency mode by fitting the absorption spectrum.

the self-consistency of our analysis. It should also be noted that the coupling of ν_3 at 1506 cm^{-1} is neglected in our fits because of its small coupling constant.

Earlier results obtained from polarized absorption measurements on single crystals of MbCN by Eaton and Hochstrasser[15] provides further experimental material to check the validity of our analysis. These authors used polarized light to measure the absorption of single crystals containing two molecules per unit cell in a $P2_1$ space group. For monoclinic type A crystals flattened on the $b \times c$ face, the light was incident to the bc crystal face with polarization parallel to either the c or b crystal axes. Thus, they determined the extinction ratio E_c/E_b as a function of wavelength. In case of a pure circular oscillator in a D_{4h} symmetry, one expects $E_x = E_y$, so that E_c/E_b is wavelength (wavenumber) independent. However, the authors obtained a significant dispersion that they interpreted as resulting from symmetry-lowering distortions. Some of their data points are depicted in the intermediate panel of Figure 4.

If the absorption profiles $E_x(\Omega)$ and $E_y(\Omega)$ in Figure 4 derived from our analysis are valid, they can be utilized to reproduce the extinction ratio E_c/E_b by means of the following equation:

$$\frac{E_c}{E_b} = \frac{n_{cx}^2 E_x(\Omega_{exc}) + n_{cy}^2 E_y(\Omega_{exc})}{n_{bx}^2 E_x(\Omega_{exc}) + n_{by}^2 E_y(\Omega_{exc})} \quad (16)$$

where the coefficients n_{bx}, n_{by}, n_{cx}, and n_{cy} are the direction cosines of c and b with respect to the x and y components of the molecular coordinate system that El Naggar et al.[33] determined for MbCN. By inserting these and the values for $E_x(\Omega_{exc})$ and $E_y(\Omega_{exc})$, we obtained the solid curve shown in the intermediate panel of Figure 4. The agreement with the experimental data is excellent between 20 000 and 25 000 cm^{-1}, whereas the calculation somewhat overestimates the ratio at higher wavenumbers. This discrepancy, however, is not surprising in view of our heuristic treatment of the small absorption band above 26 000 cm^{-1}. The agreement in the B-band region strongly corroborates the consistency and validity of our analysis.

A consistent fit to all absorption spectra measured between 20 and 300 K yields the temperature dependence of the Gaussian broadening $\sigma^2(T)$ as shown in Figure 5a. For comparison, $\sigma^2(T)$ values observed for MbCO and Mb are also depicted. The solid line reflects the fit of the harmonic model (eq 15) to the data. An onset of anharmonic motions in the low-frequency bath starts at about 130 K, somewhat lower than the solvent glass transition temperature, which is known to determine $\sigma^2(T)$ of MbCO. The contributions to $\sigma^2(T)$ due to anharmonicity ($\Delta\sigma^2(T)$, that is, the differences between the observed $\sigma^2(T)$ values and the
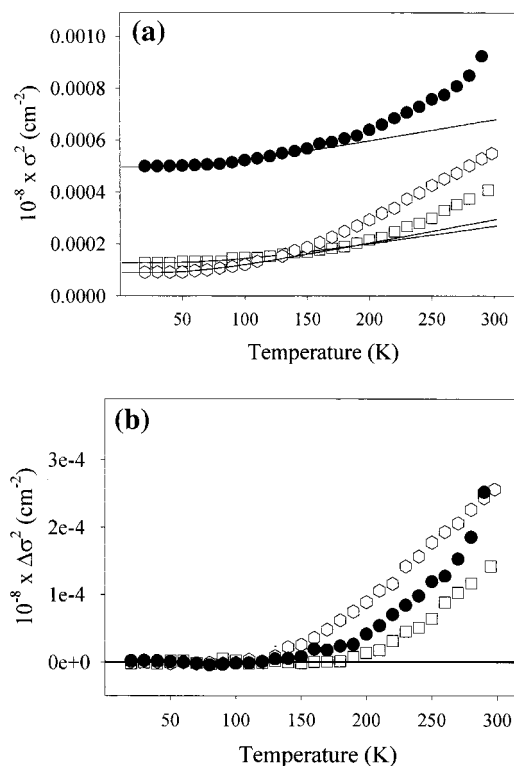

Figure 5. (a) Temperature dependence of σ^2 as derived from the Soret band-shape analysis of MbCN (●), MbCO (□) and Mb (hexagon symbol). The solid line results from fitting eq 15 to the low-temperature experimental data. (b) Temperature dependence of $\Delta\sigma^2$ values (i.e., the difference between the observed σ^2 values and the prediction of the harmonic model, eq 15); these represent the contributions of anharmonic motions to the Gaussian width of the Soret band.

predictions of the harmonic model visualized by the solid lines in Figure 5a, are displayed in Figure 5b for the three myoglobin derivatives.

By identifying the Einstein oscillator described by eqs 14−16 with the iron motion relative to the carbons of the heme skeleton, Melchers et al.[6] showed for harmonic motions that the iron mean square fluctuation depends linearly on $\sigma^2(T)$. If the same linear mapping also holds for the anharmonic contributions, Figure 5a also illustrates the temperature dependence of the iron's mean square fluctuation. Hence, the latter are substantially larger for MbCN than those for MbCO and are comparable with those observed for Mb. This is a surprising result, since one would generally expect the iron to be less mobile in a hexacoordinated conformation.

The above analysis confirms earlier results[7] indicating a comparatively strong coupling in the region between 300 and 400 cm^{-1}. The Raman spectra reveal that it arises from comparable contributions of ν_8 (344 cm^{-1}), a peripheral propionic acid deformation mode (375 cm^{-1}), and a vinyl deformation mode (411 cm^{-1}). Minor contributions are provided by the out-of-plane modes γ_6 (299 cm^{-1}) and γ_7 (327 cm^{-1}), the E_u mode ν_{50} (357 cm^{-1}), and the Fe−CN stretch (455 cm^{-1}).

Discussion

Raman Data. In-Plane Heme Distortions. Our analysis of DRD and REP of the B band has revealed that strong intrastate vibronic coupling of B_{1g} symmetry is responsible for the significant deviation of its depolarization ratio from the D_{4h} value of 0.125 when excited in the Soret band. This is a surprising result, since the ν_4 lines of deoxyMb, oxyMb[35,34] and ferrocytochrome c[36] exhibit depolarization ratios between

0.13 and 0.17. Theoretical calculations based on depolarization ratios measured between the B and Q_v bands predict a similar behavior for deoxyHbA, oxyHbA, and oxyHbA-BME[34] and deoxyHb and Hb trout IV.[11,37] The situation is different in the pre-resonance and resonance region of the Q_v band, where for most of the above molecules ν_4 displays a strong depolarization ratio dispersion with large deviations from D_{4h}.

All the heme proteins mentioned above have their iron atoms in the ferrous state. One may therefore suspect that the behavior of MbCN is due to the ferric state of its iron atom. This, however, can be ruled out on the basis of the low ρ value of the ν_4-mode of aquometMb, which exhibits 0.13 with 425-nm excitation (data not shown).[38] However, aquometMb has its iron in the high-spin state diagnostic of a weak axial ligand. In contrast, CN is a strong ligand and gives rise to a low-spin configuration. This situation is similar to horse heart ferricytochrome c, where the Met residue serves as the sixth ligand. Indeed, earlier measurements in the region between the Q_v and B bands show that the depolarization ratio of ν_4 is minimal ($\rho = 0.15$) around 21.000 cm^{-1} (476 nm) and increases with lower excitation wavelengths to reach 0.2 already at 21.838 cm^{-1} (458 nm), which is still pre-resonant with respect to the Soret transition.[39] This DPR value is reduced to 0.18 at alkaline pH because Met is replaced by a Lys in a somewhat more open heme crevice. We measured polarized Raman spectra of ferricytochrome c in resonance with the Soret transition (406 nm) and obtained $\rho(\nu_4) = 0.3$ (Unger et al., unpublished).[40] That is even larger than the values obtained for MbCN and suggests that strong axial ligands impose significant heme distortions when the iron is in the ferric configuration.

This notion is also in accordance with results from NMR and ESR experiments on high- and low-spin ferric heme complexes, which all suggest that a rhombic distortion causes the Fe^{3+} ^{2}E(d$_{xz}$, d$_{yz}$) (^{4}E for high-spin configurations) multiplet to split.[13b,c,14,41,42] Mayer and Eicher[13b] investigated the proton magnetic resonances from the methyl groups of several heme model compounds and heme proteins. They found that asymmetric distortions induced by peripheral heme substituents and the protein environment may cause an asymmetry of the iron's electron distribution, depending on the symmetry of the electronic ground state. For low-spin ferric hemes, their results are indicative of a split ^{2}E state being lowest in energy. This state is very sensitive to asymmetric electronic perturbations so that the actual symmetry of the Fe^{3+} ground state becomes C_{2v}. The situation is different in the high-spin aqueous metMb, where ^{6}A is the iron atom ground state, which is much less sensitive to asymmetric perturbations. These findings led Mayer and Eicher to conclude that the perturbation of the Fe ion's point symmetry, as imposed by the heme peripheral substituents and by heme–protein interactions, is more effective in the ferric low-spin than in the high-spin heme groups. In turn, the predicted asymmetric electron distribution of high spin Fe^{3+} certainly favors corresponding distortions of the macrocycle, as probed by the depolarization ratio of ν_4, ν_2, and ν_{10}.

The existence of rhombic (B$_{1g}$) heme distortions is confirmed by electron spin–echo envelope modulation spectroscopy on MbCN, which reveals differences in the Fe–N$_{pyrrole}$ bond lengths. This was related to the eclipsed position of the tilted proximal imidazole with respect to the Fe–N$_{pyrrole}$ vector.[14]

Whereas all the above data consistently indicate a strong distortion of ferric high-spin hemes, they do not reveal the structural origin and the pattern of the perturbation. Apparently, both axial ligands must be considered as possible candidates. CN may induce distortions by nonbonding interactions with the
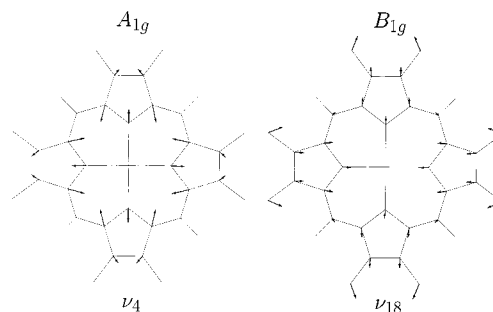

Figure 6. Cartesian eigenvectors of (a) ν_{18}(B$_{1g}$) and (b) ν_4(A$_{1g}$) of Ni(II)-octaethylporphyrin as obtained from the normal coordinate analysis by Unger et al. (manuscript in preparation).

heme group if it is tilted with respect to the heme normal. This issue is unresolved. A recent Raman study by Hirota et al.[31] suggests than CN exhibits an upright position parallel to the heme normal. On the contrary, for sperm whale Mb, the tilt angle was determined to be 13° by NMR spectroscopy[13c] and to be 21–22° by polarized IR spectroscopy on Mb single crystals.[43] Both studies agree in suggesting that the ligand projection onto the heme exhibits an azimuthal angle of ca. 35° with respect to the N–Fe–N line, so that a possible ligand–heme interaction would involve the methine carbons rather than the N-pyrroles. That would induce a B$_{2g}$-type rather than a B$_{1g}$ distortion[11] and would in particular affect the ν_3 mode, which is predominantly composed of a C$_m$–C$_\alpha$, stretch.[45] This prediction is in contrast to our Raman data (Figure 2), which clearly show that ν_3 is much less affected than ν_2 and that the distortion is of B$_{1g}$ symmetry. Hence, we exclude a direct influence of CN on the heme structure as a cause of this type of distortion. However, this ligand clearly has an indirect influence by giving rise to a low-spin ferric state of the central iron atom.

The other possible candidate for directly inducing the above B$_{1g}$-type heme distortions is the proximal histidine. This notion is consistent with the nearly eclipsed position of the imidazole with respect to the N–Fe–N line.[14] In this case, imidazole tilting gives rise to stronger nonbonding interactions between the imidazole carbons and the pyrrole nitrogens.[44] As shown earlier, such an interaction must indeed cause a B$_{1g}$ distortion, in accordance with our Raman data.[11,34] We therefore conclude that, as in ferrous hexacoordinated heme proteins,[34,36] the proximal imidazole gives rise to asymmetric heme distortions. In addition, however, the low-spin ferric state produces an asymmetric electronic distribution of the iron ground state, which in turn amplifies the macrocycle distortion.

The distortions discussed so far can be described in terms of the SNCDs $\partial\bar{Q}_a^{B_{1g}}$, which appear in the coupling matrix elements $c_{lm}^{B_{1g}}$. Jentzen et al.[18] have shown that porphyrin distortions predominantly arise from distortions along the normal coordinates of the lowest frequency modes of each symmetry block. Concerning B$_{1g}$, this is the vibration ν_{18} (168 cm^{-1}), which involves motions of the entire pyrrole group along the Fe–N$_{pyrrole}$ vectors. Opposite pyrroles move in-phase, adjacent ones out-of-phase. This is illustrated in Figure 6, which exhibits the normal coordinate of ν_{18} calculated for Ni(II)octaethylporphyrin (Unger et al., unpublished; cf. also the study by Li et al.[45]).

The above findings and interpretations are strongly corroborated by very recent NCD analyses by the Shelnutt group. These researchers have investigated the heme groups of numerous heme proteins to obtain their in-plane and out-of-plane distortions. They have also investigated two MbCN proteins from the Loggerhead sea turtle (*Caretta caretta*) and sea hare

(*Aplysia limacina*). The X-ray crystallographic structure of both proteins[46] were found to exhibit comparatively strong B_{1g} distortions for the heme groups, namely $\Delta_{B_{1g}} = \sum_j \bar{q}_j^{B_{1g}} = 0.178$ and 0.245 Å for sea turtle and sea hare, respectively.[47] As suggested above, these distortions stem, indeed, nearly entirely from deformations along the normal coordinate of the ν_{18} vibration. Distortions of B_{2g} and A_{2g} symmetry were found to be by more than a factor of 2 lower, and they are by far less statistically significant. On the contrary, a similar investigation of the aquomet form of sea turtle myoglobin revealed a $\Delta_{B_{1g}}$ of only 0.061 Å.[48] These results clearly corroborate the notion that the CN induced low-spin ferric state causes strong B_{1g} distortions of the heme macrocycle.

Out-of-Plane Heme Distortions. Thus far, the discussion has focused on in-plane modes, in line with the assumptions made for the theoretical approach (eq 6). This was based on the conventional wisdom that hexacoordinated porphyrins prefer a planar structure. Recent re-investigations of crystal structures have suggested, however, that even the heme groups in MbCO exhibit some degree of nonplanarity.[18b] The appearance of bands arising from out-of-plane vibrations shows that this also applies to MbCN. Whereas Hu et al.[27] already identified the Raman line of γ_{11} (714 cm^{-1}, B_{1u}) we additionally found two bands of A_{2u} modes at 299 (γ_6) and 327 cm^{-1} (γ_7) Raman activity of such modes requires the existence of out-of plane distortions $\delta \bar{q}_{oop}^{\Gamma_{oop}}$. For Soret excitation, the corresponding Franck−Condon type vibronic coupling is accounted for by matrix elements $\langle B_{x,y} | \partial^2 H_{el}(q,Q)/\partial Q_r dQ_{oop}^{\Gamma_{oop}} | B_{x,y} \rangle \partial \bar{Q}_{oop}^{\Gamma_{oop}} \langle 1 | Q_r | 0 \rangle$ in eq 6. Group theory dictates that $\Gamma_{oop} = A_{1u}$, B_{1u}, B_{2u}, and A_{2u}. Since the bands of the two A_{2u} modes appear polarized, the corresponding matrix element for intrastate coupling is of A_{1g} symmetry. This shows that the heme group exhibits A_{2u}-type distortions, which are generally dominated by contributions from normal deformations along the A_{2u}-type doming mode γ_9.[18] This vibration involves a significant displacement of the central metal atom and is of functional importance for the dynamics of ligand binding.[49] In accordance with the above notion, we observed a nearly depolarized Raman line for γ_{11}, consistent with the symmetry of the corresponding vibronic coupling operator, that is, $\Gamma_{oop} \otimes \Gamma_r = A_{2u} \otimes B_{1u} = B_{2g}$.

It is again illuminating to refer to the NCD studies of Shelnutt,[47] who obtained the following total out-of-plane distortions for sea turtle and sea hare MbCN, respectively: $\Delta_{A_{2u}} =$ 0.267 and 0.196 Å, $\Delta_{B_{2u}} = 0.334$ and 0.13 Å, $\Delta_{B_{1u}} = 0.19$ and 0.18 Å. These data suggest that the heme group of MbCN is indeed domed and that the extent of doming strongly depends on the protein environment. Again, the NCD analysis confirms the present data on sperm whale MbCN.

Absorption Data. We now discuss the dynamic information obtained from the temperature dependence of the optical absorption spectra. The temperature dependence of both σ^2 and E_{Bx} clearly identifies two dynamic regimes (Figure 5a and 5b). At low temperature, the system is characterized by harmonic vibrations, which can be described by an average Einstein harmonic oscillator coupled to the electronic transition (eqs 15 and 16). Parameter values that characterize this coupling are listed in Table 5, in comparison with those previously obtained for MbCO and for deoxyMb. We emphasize that it is possible to fit the low-temperature behavior of both σ^2 and ν_0 (in the range 20−150 K) with the same value for the effective frequency, namely $<\nu> = 140$ cm^{-1}. This is very close to the value of $\langle \nu \rangle = 135$ cm^{-1} obtained for deoxyMb but significantly smaller than the value of $\langle \nu \rangle = 180$ cm^{-1} obtained for MbCO. This finding is consistent with the presence of out-of-plane

TABLE 5: Values of the Parameters that Characterize the Coupling of the Soret Band with the "bath" of Low Frequency Modes in the Harmonic Regime

derivatives	NS	$\langle \nu \rangle$ (cm^{-1})	σ_{in} (cm^{-1})	$T_f(K)^a$	R^b
Mb−CN	0.4 ± 0.1	139 ± 10	200 ± 20	150	1.02 ± 0.004
Mb−CO^c	0.3 ± 0.1	180 ± 20	53 ± 38	190	1.01 ± 0.002
Mb^c	0.5 ± 0.1	135 ± 10	0	120	1.02 ± 0.004

^{a} T_f represents the temperature at which the onset of anharmonicity is detected (see Figure 5b). ^{b} R values were calculated by assuming the coupling with $N = 50$ low-frequency modes. ^{c} Parameter values relative to Mb−Co and Mb were taken from Cupane et al.[2]

distortions of the heme group in MbCN, as inferred from our Raman data from the following argument. As shown in earlier studies from our laboratories,[5,9] vibrational motions involving the central metal atom provide a dominant contribution to the Einstein oscillator and are pivotal for the occurrence of deviations from the harmonic behavior above the glass temperature. In D_{4h} symmetry, these motions must be part of normal vibrations of the macrocycle having either E_u (in-plane) or A_{2u} (out-of-plane) symmetry. For such modes, vibronic transitions into the B state, which involves an odd number of vibrational quanta, are symmetry forbidden, whereas those involving an even number are allowed, so that only $0 \rightarrow 2$ transitions may contribute to the Soret absorption. However, in the presence of A_{2u}-type (doming) distortions that effectively lower the symmetry from D_{4h} to D_4, out-of-plane modes of A_{2u} symmetry become Franck−Condon active even for $0 \rightarrow 1$ transitions. Compared with a heme in a nearly planar configuration (e.g., MbCO) this gives rise to a lowering of the effective frequency $\langle \nu \rangle$, as observed.

Furthermore, MbCN is characterized by a much larger value of σ_{in} as compared to that for MbCO. This reflects an increased spectral heterogeneity of the former, likely related to the disorder of angular coordinates of the bound CN with respect to the heme normal[43] and/or to structural disorder of the heme macrocycle (i.e., a distribution of the out-of-plane and rhombic porphyrin distortions). The iron−porphyrin mean-square fluctuation reflected by $\sigma(T)$ in Figure 5a show clear deviations from the harmonic behavior, which appears at high temperatures. Such deviations can be attributed to motions of the protein matrix that become certainly anharmonic at high temperatures and that are coupled to the heme either via the covalent bond between the iron and the proximal histidine or via nonbonded interactions with the side chains of amino acids of the distal and/or proximal heme pocket.[5,9] A recent investigation of various metal−octaethylporphyrins dissolved in organic solvents[9] showed that the coupling between metalloporphyrin and solvent motions (a) can be very effective even though it is only constituted by nonbonded interactions and (b) depends dramatically on the size of the central metal, that is, upon the strength of the ligand field imposed by the four pyrrole nitrogens. The data exhibited in Figure 5 show that while the mean square fluctuation for MbCN is between the values for deoxyMb and MbCO below 200 K, it becomes equal to or even slightly larger than the deoxyMb values at room temperature. This is a surprising result, since one generally expects the iron to be less mobile in a hexacoordinated conformation.[50] In view of the above discussion, we tentatively attribute the observed behavior of MbCN to the following effects: (1) doming of the heme group, which couples the anharmonic out-of-plane motions more effectively to the Soret transition, (2) the presence of the CN$^-$ ligand that transmits motions of the distal histidine to the central iron atom, and (3) a larger intrinsic mobility of ligated Fe^{3+} compared with Fe^{2+} in the hexacoordinated state. More experimental work on

Anharmonic Protein Motions and Heme Deformations

J. Phys. Chem. B, Vol. 104, No. 19, 2000 **4763**

different heme proteins with different ligands and/or oxidation states, as well as on model systems, is required to assess the relative contributions of the aforementioned effects.

List of Abbreviations

DRD, depolarization ratio dispersion; SNCD, static normal coordinate deformation; REP, resonance excitation profile; KHD, Kramers−Heisenberg-Dirac equation; FC, Franck− Condon; JT, Jahn−Teller.

References and Notes

(1) Frauenfelder, H.; Petsko, G. A.; Tsernoglou, D. *Nature* **1979,** *280*, 558. Elber, R.; Karplus, M. *Science* **1987**, *235*, 318. Frauenfelder, H.; Parak, F.; Young, R. D. *Annu. Rev. Biophys. Biophys. Chem.* **1988**, *17*, 451.

(2) Cupane, A.; Leone, M.; Vitrano, E.; Cordone, L. E. *Biophys. J.* **1995**, *23*, 385.

(3) Markam, J. J. *Rev. Mod. Phys.* **1959**, *31*, 956.

(4) DiPace, A.; Cupane, A.; Leone, M.; Vitrano, E.; Cordone, L. *Biophys. J.* **1992**, *63*, 475. Cupane, A.; Leone, M.; Vitrano, E. *Eur. Biophys. J.* **1993**, *21*, 385.

(5) Leone, M.; Cupane, A.; Militello, V.; Cordone, L. *Eur. Biophys. J.* **1994**, *23*, 349.

(6) Melchers, B.; Knapp, E. W.; Parak, F.; Cordone, L.; Cupane, A.; Leone, M. *Biophys. J.* **1996**, 70, 2092.

(7) Leone, M.; Cupane, A.; Cordone, L. *Eur. Biophys. J.* **1996**, *24*, 117.

(8) Hu, S.; Morris, I. K.; Singh, S. P.; Smith, K. M.; Spiro, T. G. *J. Am. Chem. Soc.* **1993**, *115*, 12466.

(9) Cupane, A.; Leone, M.; Cordone, L.; Gilch, H.; Dreybrodt, W.; Unger, E.; Schweitzer-Stenner, R. *J. Phys. Chem.* **1996**, *100*, 14192. Cupane, A.; Leone, M.; Unger, E.; Lemke, C.; Beck, M.; Dreybrodt, W.; Schweitzer-Stenner, R. *J. Phys. Chem. B.* **1998**, *102*, 6612.

(10) Doster, W.; Cusack, S.; Petry, W. *Nature (London)* **1989**, *337*, 754.

(11) Schweitzer-Stenner, R. *Q. Rev. Biophys.* **1989**, *22*, 381.

(12) Unger, E.; Bobinger, U.; Dreybrodt, W.; Schweitzer-Stenner, R. *J. Phys. Chem.* **1993**, *97*, 9956. Schweitzer-Stenner, R.; Stichternath, A.; Dreybrodt, W.; Jentzen, W.; Song, X.-Z.; Shelnutt, J. A.; Faurskov-Nielsen, O.; Medforth, C.; Smith, K. M. *J. Chem. Phys.* **1997**, *107*, 1794.

(13) Budd, D. L.; La Mar, G. N.; Langry, K. C.; Smith, K. M.; Nayyir-Mazhir, R. *J. Am. Chem. Soc.* **1979**, *101*, 6091. Mayer, A.; Eicher, H. *J. Mol. Catal.* **1984**, *23*, 151. (c) Emerson, S. D.; LaMar, G. N. *Biochemistry* **1990**, *29*, 1556.

(14) Magliozzo, R. S.; Peisach, J. *Biochemistry* **1993**, *32*, 8446.

(15) Eaton, W. A.; Hochstrasser, R. M. *J. Chem. Phys.* **1968**, *49*, 985.

(16) Gouterman, M. *J. Chem. Phys.* **1959**, *30*, 1139

(17) Zgierski, M. Z.; Pawlikowski, M. *Chem. Phys.* **1982**, *65*, 335.

(18) Jentzen, W.; Song, X.-Z.; Shelnutt, J. A. *J. Phys. Chem. B.* **1997**, *101*, 1684. Jentzen, W.; Ma, J.-G.; Shelnutt, J. A. *Biophys. J.* **1998**, *74*, 753.

(19) Raman spectra taken with Soret excitation predominantly contain bands the intensities of which stem from intramanifold A_{1g}-type (Franck− Condon) and to a minor extent from B_{1g}-type (Jahn Teller) coupling. In the Raman tensor, the corresponding vibronic coupling elements are weighted with the square of the strong electronic dipole moment M_g^B of the Soret band. As a consequence, interferences with terms from intermanifold Herzberg−Teller coupling between Q and B states do not significantly influence the Raman cross section, since the latter is weighted with the product of M_g^B and the much weaker transition moment M_g^Q of the Q band. The situation is qualitatively different for Q-state scattering, where multiple interference effects between different coupling processes, as well as multimode mixing, occurs. This complicates the theoretical treatment and requires the full consideration of all states of the four orbital model.[13b]

(20) A_{1g} distortions do not alter the molecule's symmetry. They are normally defined with respect to a molecular configuration, for which $|Q\rangle$ and $|B\rangle$ are determined by a 50:50 mixing of the configurations $|a_{1u}e_g\rangle$ and $|a_{2u}e_g\rangle$.

(21) For sake of simplicity, the following matrix elements are expressed in terms of the basis functions $|Q_x\rangle$, $|Q_y\rangle$, $|B_x\rangle$, and $|B_y\rangle$ of the undistorted molecule. In the electronic basis of a molecule affected by B_{1g}-type electronic distortions $c_{Im}^{B_{1g}}$ is unequal to zero due to product terms $(\partial H_{el0}(q,Q))/\partial Q_r^{A_{1g}}[(\partial H_{el0}(q,Q)/dQ_a^{B_{1g}})/(E_Q - E_B)\partial \bar{Q}_a^{B_{1g}} Q_r^{A_{1g}}$. A complete listing of the matrix elements are given by Bobinger et al.[22] These terms are explicitly accounted for in the computer program used to analyze our Raman data. Their contributions, however, are significant only in the case of very strong electronic perturbations, which are not operative in normal porphyrins.

(22) Bobinger, U.; Schweitzer-Stenner, R.; Dreybrodt, W. *J. Raman Spectrosc.* **1989**, *10*, 191.

(23) Cordone, L.; Cupane, A.; Leone, M.; Vitrano, E. *Biophys. Chem.* **1986**, *24*, 259.

(24) Jentzen, W.; Unger, E.; Karvounis, G.; Shelnutt, J. A.; Dreybrodt, W.; Schweitzer-Stenner, R. *J. Phys. Chem.* **1996**, *100*, 14184. Unger, E.; Dreybrodt, W.; Schweitzer-Stenner, R. *J. Phys. Chem. B.* **1997**, *101*, 5997.

(25) Dreybrodt, W.; Stichternath, A. *Proceedings of the XIV− International Conference on Raman Spectroscopy; Hong Kong;* Yu, N. T., Li, X.-Y. Eds.; Wiley & Sons: New York, 1994, p 1066.

(26) Stallard, B.; Champion, P. M.; Callis, P. R.; Albrecht, A. C. *J. Chem. Phys.* **1983**, *78*, 712. Stallard, B. R.; Callis, P. R.; Champion, P. M.; Albrecht, A. C. *J. Chem. Phys.* **1984,** *89*, 70.

(27) Hu, S.; Smith, K. M.; Spiro, T. G. *J. Am. Chem. Soc.* **1996**, *118*, 12638.

(28) Smulevich, G.; Hu, S.; Rodger, K. R.; Goodin, D. B.; Smith, K. M.; Spiro, T. G. *Biospectrosc.* **1996**, *2*, 365.

(29) Czernuszewicz, R.; Li, X. Y.; Spiro, T. G. *J. Am. Chem. Soc.* **1989**, *111*, 7024.

(30) Gottfried, D. S.; Peterson, E. S.; Sheikh, A. G.; Wang, J.; Yang, J.; Friedman, J. M. *J. Phys. Chem.* **1996**, *100*, 12034.

(31) Hirota, S.; Ogura, T.; Shinazawa-Itoh, K.; Yoshikawa, S.; Kitagawa, T. *J. Phys. Chem* **1996,** 100, 15274.

(32) Lemke, C.; Dreybrodt, W.; Shelnutt, J. A.; Quirke, J. M. E.; Schweitzer-Stenner, R. *J. Raman Spectrosc.* **1998**, *29*, 945.

(33) El Naggar, S.; Schweitzer-Stenner, R.; Dreybrodt, W.; Mayer, A. *Biophys. Struct. Mech.* **1984,** *10*, 257.

(34) Schweitzer-Stenner, R.; Dreybrodt, W. *J. Raman Spectrosc.* **1992**, *23*, 539.

(35) Bangcharoenpaurpong, O.; Schomaker, K. T.; Champion, P. M. *J. Am. Chem. Soc.* **1984**, *106*, 4701.

(36) Schweitzer-Stenner, R.; Bobinger, U.; Dreybrodt, W. *J. Raman Spectrosc.* **1991**, *22*, 65.

(37) Schweitzer-Stenner, R.; Bosenbeck, M.; Dreybrodt, W. *Biophys. J.* **1993**, *64*, 1194.

(38) This seems to contradict results from polarized absorption measurements on single crystals reported in ref 16, which show a strong dispersion of the E_c/E_b ratio in the Soret band region. However, this could well result mostly from pure electronic B_{1g}-type splitting, which has a very limited impact on the DPR in the B-band region. Moreover, the E_c/E_b dispersion can be expected to be more pronounced for B_x and B_y bands with smaller halfwidths, as it is the case for aquometMb.

(39) Kubitscheck, U.; Dreybrodt, W.; Schweitzer-Stenner, R. *Spectrosc. Lett.* **1986**, *19*, 681.

(40) Stallard et al.[26] have measured a much lower depolarization ratio of 0.14 with 413-nm excitation. Their result is also at odds with earlier depolarization ratio measurements in the visible region, which clearly indicate an increase of the depolarization ratio of ν_4 towards B-band excitation.[39]

(41) LaMar, G.; Viscio, D. B.; Smith, K. M.; Caughey, W. S.; Smith, M. L. *J. Am. Chem. Soc.* **1978**, *100*, 8084.

(42) Mitra, S. Magnetic Susceptibility of Iron Porphyrins. In: *Iron Porphyrins*, Part II; Lever, A. B. P., Gray, H. B., Eds.; Addison-Wesley: London, 1983; pp 1−42.

(43) Sage, J. T. *Appl. Spectrosc.* **1997**, *51*, 568.

(44) Gellin, B. R.; Karplus, M. *Proc. Natl. Acad. Sci. U.S.A.* **1977**, *74*, 801.

(45) Li, X.-Y.; Czernuszewicz, R. S.; Kincaid, J. R.; Stein, P. R.; Spiro, T. G. *J. Phys. Chem.* **1990**, *94*, 47.

(46) (a) Nardini, M.; Tarricone, C.; Rizzi, M.; Lania, A.; Desideri, A.; De Sanctis, G.; Coletta, M.; Petruzzelli, R.; Ascenzi, P.; Coda, A.; Bolognesi, M. *Protein Data Bank* **1995**, 1LHT. Conti, E.; Moser, C.; Rizzi, M.; Mattevi, A.; Lionetti, C.; Coda, A.; Asceni, P.; Brunori, M.; Bolognesi, M. *Protein Data Bank* **1995**, 2FAL.

(47) Shelnutt, J. A. In *The Porphyrin Handbook*; (Kadish, K. M., Smith, K. M., Guilard, R., Eds.; Academic Press: London, 2000; Vol. 7, Chapter 50, pp 167−223. The data may also be obtained from Dr. Shelnutt's web side: http://jasheln.unm.edu.

(48) Nardini, M.; Tarricone, C.; Rizzi, M.; Lania, A.; Desideri, A.; De Sanctis, G.; Coletta, M.; Petruzzelli, R.; Ascenzi, P.; Coda, A.; Bolognesi, M. *Protein Data Bank* **1995**, 1LHS.

(49) Zhu, L.; Sage, J. T.; Champion, M. *Science* **1994**, *266*, 629.
(50) Šrajer, V.; Reinish, L.; Champion, P. M. *J. Am. Chem. Soc.* **1988**, *110*, 6656.